Letters

An L2C2 Resonant Converter With Reduced Components and Wide Gain Range

Jianglin Nie, Jiajin Li, Georgios Konstantinou, *Senior Member, IEEE*, Yuhao Deng, Zeyao Hu, and Zeliang Shu, *Senior Member, IEEE*

***Abstract*—This letter proposes an L2C2 resonant converter that offers an extended gain range, addressing the gain limitations of the widely adopted *LLC* converter. Compared to other wide-gain-range resonant converters, the proposed topology requires only one additional resonant capacitor beyond the *LLC* converter, resulting in lower cost, higher reliability, and improved efficiency. The proposed topology exhibits a unique characteristic that a larger magnetizing inductance leads to a wider gain range. As a result, increased magnetizing inductance contributes to both higher efficiency and broader gain adaptability. The operation and effectiveness of the proposed converter are validated through an experimental prototype achieving a peak efficiency of 96.5% with an output voltage range from 24 to 120 V.**

***Index Terms*—L2C2 converter, larger magnetizing inductance, low component count, wide gain range.**

I. Introduction

THE traditional *LLC* resonant converter has been widely adopted in diverse applications such as renewable energy systems, electric vehicle onboard chargers, and compact consumer electronics, due to its strong soft-switching capability, inherent ability to eliminate transformer dc bias, and simple structure [1]. However, its relatively narrow voltage gain range limits its applicability.

To address this limitation, various improvements to the *LLC* converter have been proposed [1], [2], [3], [4], [5]. In [1] and [1], multilevel modes are introduced using dual- and full-bridge structures, enabling port voltage modulation via multiple switches and transformers. Voltage-doubling rectifiers with adjustable gain through added switches are adopted in [3] and [4]. In [5], a hybrid *LLC* converter integrates a nonisolated buck–boost stage, forming a cascaded structure that extends the *LLC*'s input voltage range. Although these topologies enable wide gain ranges, they typically require extra switches, transformers, and resonant tanks, which increase cost, size, and reduce efficiency and reliability.

To address these issues, several studies have modified only the *LLC* resonant tank, without adding extra switches or diodes [6], [7], [8], [9], [10], [11]. Most adopt notch filters composed of parallel *LC* branches to introduce a resonant point and extend the gain range [6], [7], [8], [9]. However, the zero-voltage switching (ZVS) performance of such filters is generally poor, often requiring extra series capacitors or magnetic elements. Series *LC* tanks have also been proposed to reduce component count, but their gain range remains limited [10], [11].

In summary, while many resonant topologies with extended gain range have been proposed, most still suffer from too many uses of inductors, transformers, capacitors, switches, and diodes. This compromises cost, efficiency, and reliability, making these solutions difficult to commercialize at scale.

To address these limitations, this letter proposes a novel L2C2 resonant converter. As shown in Fig. 1(b), the converter achieves a wide gain range, defined as the ratio of the maximum to minimum input/output voltages ($V_{\max}/V_{\min}$), while maintaining a minimal component count. The key characteristics of the topology are as follows:

1) *Wide gain range:* The proposed topology achieves a wider gain range than most modified resonant converters.

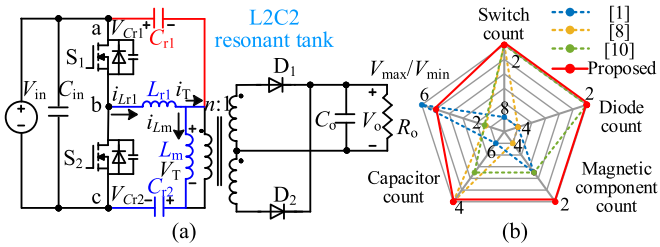

Fig. 1. Proposed L2C2 converter. (a) Topology. (b) Comparisons.

Received 11 May 2025; revised 15 June 2025; accepted 8 July 2025. Date of publication 14 July 2025; date of current version 27 August 2025. This work was supported in part by the National Key R&D Program of China under Grant 2021YFB2601500, in part by the National Natural Science Foundation of China under Grant 52077183, and in part by the Doctoral Innovation Fund Program of Southwest Jiaotong University under Grant CX-2025ZD02. *(Corresponding author: Zeliang Shu.)*

Jianglin Nie, Yuhao Deng, and Zeyao Hu are with the School of Electrical Engineering, Southwest Jiaotong University, Chengdu 611756, China (e-mail: jacksonen@my.swjtu.edu.cn; yh_deng@my.swjtu.edu.cn; zey.hu@my.swjtu.edu.cn).

Jiajin Li is with the College of Electrical Engineering, Sichuan University, Chengdu 610065, China (e-mail: 2018112018@my.swjtu.edu.cn).

Georgios Konstantinou is with the School of Electrical Engineering and Telecommunications, University of New South Wales Sydney, Sydney NSW 2052, Australia (e-mail: g.konstantinou@unsw.edu.au).

Zeliang Shu is with the School of Electrical Engineering, Southwest Jiaotong University, Chengdu 611756, China, and also with the Key Laboratory of Magnetic Suspension Technology and Maglev Vehicle, Ministry of Education, Southwest Jiaotong University, Chengdu 611756, China (e-mail: shuzeliang@swjtu.edu.cn).

Color versions of one or more figures in this article are available at https://doi.org/10.1109/TPEL.2025.3588120.

Digital Object Identifier 10.1109/TPEL.2025.3588120

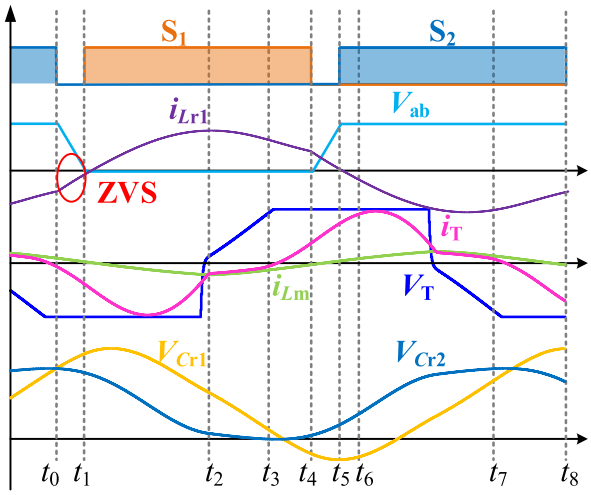

Fig. 2. Key operating waveforms.

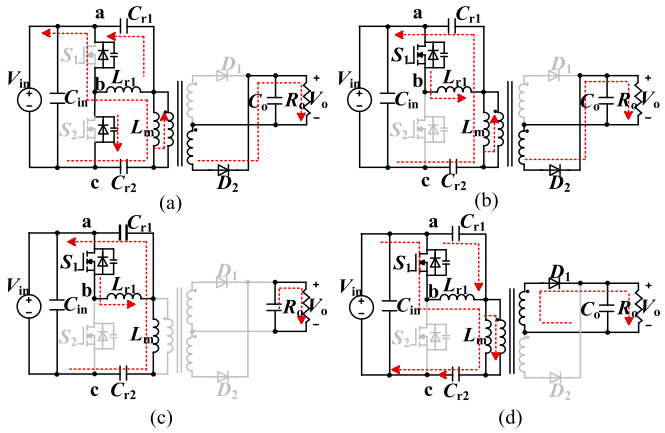

Fig. 3. Operating stages within a half switching period. (a) Stage 1[t_0–t_1). (b) Stage 2 [t_1–t_2). (c) Stage 3 [t_2–t_3). (d) Stage 4 [t_3–t_4).

2) *Minimal component overhead:* Only one extra resonant capacitor is added compared to the traditional *LLC* converter.
3) *Improved efficiency:* A larger magnetizing inductance reduces transformer losses and improves the efficiency.
4) *Easy implementation:* The design is compatible with existing *LLC* systems, allowing for easy modification.

II. Topology and Working Principle

Fig. 1(a) shows the topology of the proposed L2C2 resonant converter. The resonant tank consists of a resonant inductor L_{r1}, two capacitors C_{r1} and C_{r2}, and the transformer's magnetizing inductance L_m. Compared to the conventional *LLC* converter, the proposed topology only introduces an additional resonant capacitor C_{r2} between the positive terminal of the input voltage source $V_{\rm in}$ and the transformer. This modification requires no significant structural changes and can be easily incorporated into existing *LLC* modules or designs.

The waveforms of the proposed L2C2 converter during one switching period T_s are shown in Fig. 2, and the corresponding operating stages within a half switching cycle are in Fig. 3. As defined in Fig. 1, $i_{\rm Lr1}$ and $i_{\rm Lm}$ represent the currents through

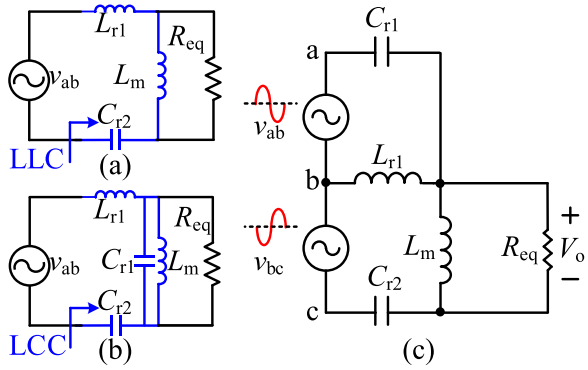

Fig. 4. FHA equivalent circuits. (a) *LLC* converter. (b) *LCC* converter. (c) L2C2 converter.

the resonant inductor L_{r1} and magnetizing inductor L_m, respectively. $V_{\rm ab}$, $V_{\rm Cr1}$, and $V_{\rm Cr2}$ denote the voltages across port ab, C_{r1}, and C_{r2}, respectively. All reference directions are consistent with those in Fig. 1.

Stage 1 [t_0, t_1): At t_0, the converter enters the dead time interval, the current $i_{\rm Lr1}$ discharges the parasitic capacitance of S_1 and charges that of S_2, resulting in a gradual transition of the port voltage $V_{\rm ab}$ from a high level to zero.

Stage 2 [t_1, t_2): At t_1, S_1 is turned-ON under ZVS. L_m is clamped by the output voltage, such that the voltage across L_m equals $-nV_{\rm o}$, where n is the turns ratio of the transformer and $V_{\rm o}$ is the output voltage. From t_0 to t_2, the transformer continuously delivers energy to the secondary side, keeping diode D_2 conducting. The magnetizing inductor voltage V_T are, thus, clamped to $-nV_{\rm o}$.

Stage 3 [t_2, t_3): At t_2, the transformer ceases energy transfer. The magnetizing inductor L_m is released from clamping and begins to resonate with C_{r1}, C_{r2}, and L_{r1}, similar to the subresonant region operation in traditional *LLC* converters. As a result, diode D_2 turns OFF. During this process, the voltages across C_{r1} and C_{r2} gradually decrease, while V_T slowly rises.

Stage 4 [t_3, t_4): At t_3, when the voltage V_T exceeds $nV_{\rm o}$, diode D_1 conducts. This reclamps L_m to the output voltage $V_{\rm o}$ and disconnects it from the resonant tank.

Subsequently, during the interval t_4–t_8, S_2 turns ON under ZVS conditions. The operation during this interval is symmetrical to t_0–t_4 and follows a similar sequence of states.

III. Design Consideration

A. Voltage Gain

The key reason for the proposed converter's extended gain range lies in its modified first harmonic approximation (FHA) equivalent circuit. As shown in Fig. 4(c), the variables $v_{\rm ab}$ and $v_{\rm bc}$ represent the fundamental components of the port voltages $V_{\rm ab}$ and $V_{\rm bc}$, respectively, obtained through Fourier decomposition. Their expressions are given in the following equation:

$$v_{\rm ab}(t)=2V_{\rm in}\sin(2\pi f_s t)/\pi,\ v_{\rm bc}(t)=-2V_{\rm in}\sin(2\pi f_s t)/\pi. \quad (1)$$

The variable $R_{\rm eq}$ represents the equivalent resistance of the output load $R_{\rm o}$ under FHA, and its expression is $R_{\rm eq}=8n^2R_{\rm o}/\pi^2$.

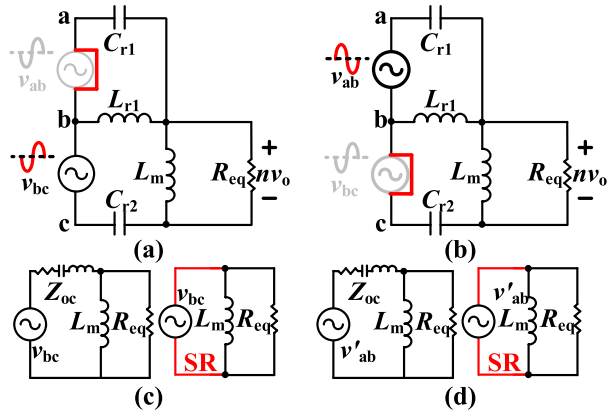

Fig. 5. FHA equivalent circuit of the L2C2 under superposition. (a) Only v_{bc}. (b) Only v_{ab}.(c) SR circuit with only v_{bc}. (d) SR circuit with only v_{ab}.

As shown in Fig. 4, unlike *LLC* and *LCC* converters that include only a single equivalent voltage source in the FHA model, the proposed converter introduces an additional resonant capacitor C_{r1}, which enables a second voltage source in the equivalent circuits.

As illustrated in Fig. 5, the principle of superposition is applied to analyze the converter's operation when either v_{bc} or v_{ab} is acting independently. The corresponding FHA equivalent circuits are shown in Fig. 5(a) and (b). Taking L_m as the reference port, Thevenin equivalent circuits can be derived for both scenarios, as shown in Fig. 5(c) and (d).

Let ω_s be the angular frequency, defined as $\omega_s = 2\pi f_s$, where f_s is the switching frequency. As shown in Fig. 5(c), the equivalent impedance Z_{oc} is given by

$$Z_{oc} = j\omega_s L_{r1} // \frac{1}{j\omega_s C_{r1}} + \frac{1}{j\omega_s C_{r2}}. \tag{2}$$

The series resonant frequency f_r of Z_{oc} is

$$f_r = 1/\left[2\pi\sqrt{L_{r1}(C_{r1}+C_{r2})}\right]. \tag{3}$$

When $f_s = f_r$, the converter operates in a series resonance (SR) and $Z_{oc} = 0$. In this case, the voltage source v_{bc} directly supplies energy to the equivalent load R_{eq}.

In Fig. 5(d), the impedance Z_{oc} shares the same expression as in (2). The equivalent voltage source corresponding to v_{ab} is denoted as v'_{ab}, and its expression is given by

$$v'_{ab} = \frac{\omega_s^2 L_{r1} C_{r1} v_{ab}}{\omega_s^2 L_{r1} C_{r1} - 1}. \tag{4}$$

Therefore, when $f_s = f_r$, the total output voltage of the circuit is the superposition of the magnitudes of v'_{ab} and v_{bc}, and the corresponding base gain is given by $M_{base} = V_o/V_{in}$ as follows:

$$M_{base} = \frac{0.5V_{in}}{n}\frac{2\omega_s^2 L_{r1} C_{r1} - 1}{\omega_s^2 L_{r1} C_{r1} - 1}. \tag{5}$$

As shown in Fig. 6, both half-bridge *LLC* and *LCC* have a base gain of $M'_{base} = 0.5V_{in}/n$, while the L2C2 converter achieves a higher base gain ($M_{base} > M'_{base}$), thereby naturally extending its achievable gain range.

The voltage gain of the proposed L2C2 converter is further derived based on the fundamental harmonic model in Fig. 5. As

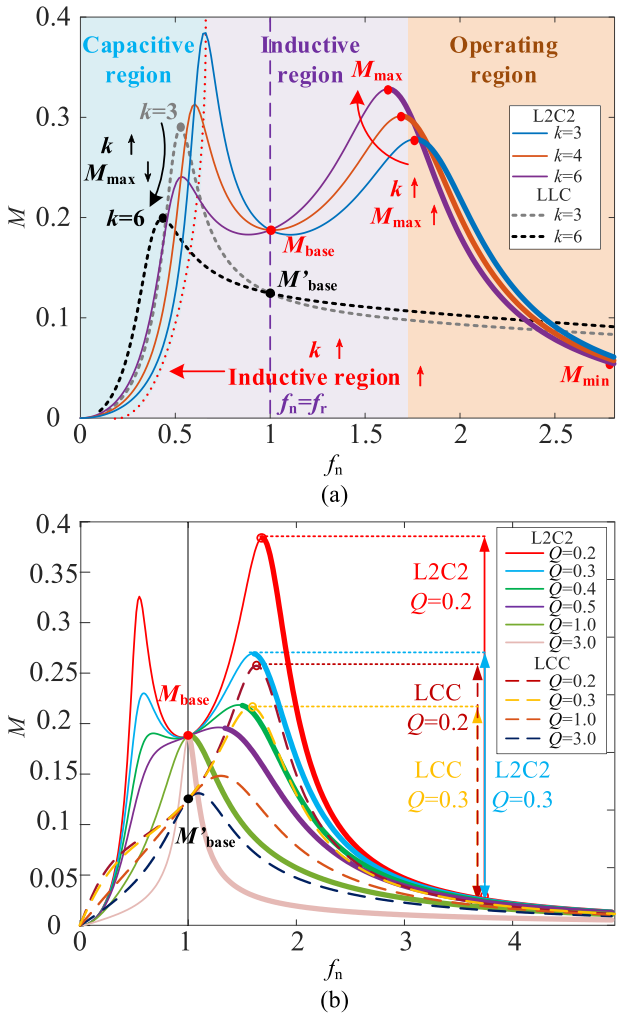

Fig. 6. Gain characteristics. (a) L2C2 and *LLC* Under varying k, with Q=0.3. (b) L2C2 and *LCC* under varying Q, with k=5.

shown in Fig. 5(a), the corresponding transfer function $H_1 = nv_o/v_{bc}$ is given by the following equation:

$$H_1 = \frac{j\omega_s L_m // R_{eq}}{(1/j\omega_s C_{r2} + 1/j\omega_s C_{r1} // j\omega_s L_{r1} + j\omega_s L_m // R_{eq})}. \tag{6}$$

When only v_{ab} is active, the corresponding transfer function $H_2 = v_o/v_{ab}$ can be derived similarly to H_1.

The expressions for the quality factor Q, the capacitor ratio λ, the inductance ratio k, and the normalized angular frequency $\omega_n = f_n = f_s/f_r$ are given in the following equation:

$$Q = \frac{1}{R_{eq}}\sqrt{\frac{L_{r1}}{C_{r2}}}, \lambda = \frac{C_{r1}}{C_{r2}}, k = \frac{L_m}{L_{r1}}, \omega_n = \omega_s\sqrt{L_{r1}C_{r1}}. \tag{7}$$

By combining Fig. 5 and (6), (7), the voltage gain $M = V_o/V_{in}$ can be derived, as shown in the following equation:

$$M = \frac{\sqrt{2}k}{n\pi \cdot \sqrt{1+(kQ\omega_n)^2} \cdot (\omega_n{}^2(\lambda+1) - \lambda - \omega_n{}^2 k + k)}. \tag{8}$$

Fig. 6(a) illustrates the voltage gain M curves under different values of f_n and k, with fixed parameters $Q = 0.3$ and $\lambda = 0.7$. Similar to conventional *LLC* converters, the impedance of

the resonant tank in the proposed topology varies with switching frequency. When the imaginary part of the impedance is positive, the circuit operates in the inductive region, where the current lags behind the voltage, allowing ZVS. In contrast, when the imaginary part is negative, the circuit enters the capacitive region, where the current leads the voltage and ZVS cannot be achieved.

Therefore, like *LLC* converters, the proposed L2C2 converter is primarily designed to operate in the inductive region. In addition, to achieve a wide gain range, the operating region of L2C2 lies in the monotonically decreasing segment of the gain curve, similar to that of *LCC* converters.

In a conventional *LLC* converter, the maximum gain $M_{\max}$ decreases rapidly as the magnetizing inductance L_m or the ratio k increases, which narrows the overall gain range. In contrast, the proposed L2C2 converter exhibits the opposite trend—$M_{\max}$ increases with k, thereby expanding the gain range of the operating region. A larger L_m not only broadens the gain range but also significantly reduces the transformer's core loss under light-load conditions and suppresses circulating current. Moreover, an increase in k extends the inductive region of the impedance characteristic, thereby enhancing the converter's ZVS capability.

Fig. 6(b) illustrates the relationship between M and f_n for different Q, under the fixed condition of $k = 5$. Regardless of the value of Q, the gain range of the conventional *LCC* converter remains narrower than that of the proposed L2C2 converter. Based on Fig. 6, the key parameters of the L2C2 converter, including the ratio k, quality factor Q, and the parameter λ, can be selected according to the desired switching frequency range and gain requirements.

B. Analysis of the ZVS Realization

Due to the short dead time, the current flowing through the switches, i_{Lr1}, can be approximated as constant during the dead time T_{dead}. Let i_{ZVS} be the minimum current required for achieving ZVS, and C_{oss} be the output parasitic capacitance of switches S_1 and S_2. The ZVS condition can be expressed as

$$i_{\text{ZVS}} T_{\text{dead}} \geq 2C_{\text{oss}} V_{\text{in}}. \tag{9}$$

Based on the FHA equivalent circuit shown in Fig. 5 and combining (8) and (9), the expression for i_{Lr} can be obtained. By setting $t = 0$, the ZVS current i_{ZVS} can be approximated as

$$i_{\text{ZVS}} = i_{Lr1}(0) = \frac{nV_o T_s}{8L_m}. \tag{10}$$

Combining (9) and (10), the ZVS condition of the proposed converter is obtained as

$$L_m \leq \frac{nT_{\text{dead}} M}{16C_{\text{oss}} f_s}. \tag{11}$$

Like the conventional *LLC* converter, the proposed L2C2 converter also enables ZVS by adjusting L_m. However, as shown in Fig. 5, the L2C2 converter allows L_m to be chosen as large as possible while still satisfying the ZVS condition in (11). This provides a wider gain range, lower transformer core loss, and reduced circulating current. In contrast, the conventional *LLC* converter and most resonant converters must compromise between ZVS and gain range, limiting the maximum value of L_m.

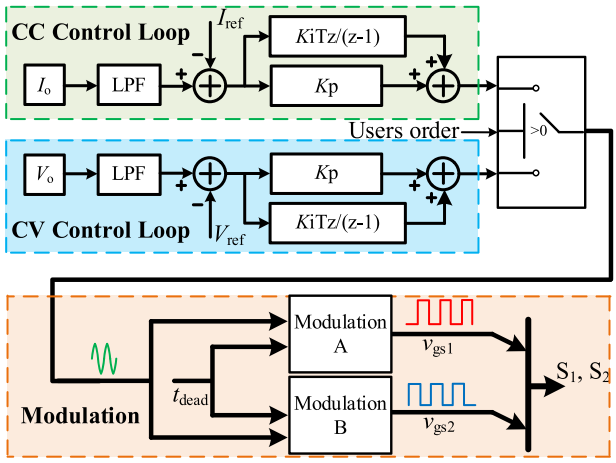

Fig. 7. Overall control block diagram of the proposed converter.

C. Control Design

The entire control system is implemented on an FPGA platform. Output voltage and current are sampled via ADCs, and the switching frequency of the converter is adjusted through a PI controller and a voltage-controlled oscillator (VCO).

As shown in Fig. 7, the converter adopts a pulse frequency modulation (PFM) architecture, consisting of three main parts: a constant voltage (CV) control loop, a constant current (CC) control loop, and a modulation module.

Taking the CV loop as an example: The output voltage V_{o} is filtered by a low-pass filter and compared with the reference voltage V_{ref}. The resulting error is processed by a PI controller. The output of the PI controller is then limited within a predefined frequency range and used as the control input of a VCO. The VCO generates a cosine carrier signal whose frequency varies according to the PI output. This carrier is then passed to modulation blocks A and B.

In the modulation blocks, the carrier is compared with fixed-threshold signals to generate complementary gate drive signals v_{gs1} and v_{gs2}, with a fixed duty ratio and programmable dead time t_{dead}.

Depending on the user-specified regulation mode, either the CV or CC loop is activated to maintain the desired output characteristics. The overall system ensures accurate output regulation across a wide voltage range by dynamically adjusting the switching frequency via PFM.

IV. Experimental Results

A 720 W experimental prototype was developed to verify the effectiveness of the proposed converter. The key parameters and components are presented in Fig. 8 and Table I, respectively. Polypropylene film capacitors (CBB type) were selected for the resonant capacitor due to their favorable high-frequency characteristics and low equivalent series resistance, making them well-suited for resonant applications. The converter adopts an FPGA to regulate V_{o} through PFM.

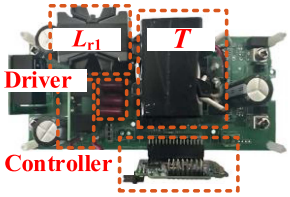

KEY PARAMETERS OF CONVERTERS

Symbol	Quantity	Parameter
V_{in}/V_o	Input/output voltage	400/24 – 120 V
f_s	Switching frequency	120 – 200 kHz
L_{r1}	Resonant inductor	100 uH
L_m	Magnetizing inductor	600 uH
C_{r1}/C_{r2}	Resonant capacitor	20/30 nF
P_o	Nominal power	720 W
n	Turns ratio	4

Fig. 8. Prototype and key parameters of proposed converter.

TABLE I
KEY COMPONENTS FOR PROPOSED CONVERTERS PROTOTYPE

Component	Components type	Amount
S_1–S_2 switches	SiC MOSFET: P3M0606K3	2
D_1–D_2 diodes	Schottky diodes: VS-30CPH03-N3	2
T magnetic core	Mn–Zn ferrite: PQ50/50 PC95	1
L_r magnetic core	Mn–Zn ferrite: PQ40/40 PC95	1
C_{r1} capacitors	10 nF CBB: PS103J3C1502	2
C_{r2} capacitors	10 nF CBB: PS103J3C1502	3
C_{in} capacitor	470 uF: CL471MVJ60BP	1
C_{out} capacitors	470 uF: ELH2DM471O35KT	2

Fig. 9 shows the steady-state experimental waveforms of the proposed converter operating with a load resistance of $R_o = 18\ \Omega$, $Q = 0.25$. As observed in Fig. 9(a) and (c), the key waveforms are consistent with those shown in Fig. 2, and the output voltage range reaches $V_{max}/V_{min} = 5$. The ZVS waveforms at the maximum and minimum output voltages are illustrated in Fig. 9(b) and (d), respectively. It can be seen that the drain-source voltage $V_{ds(S1)}$ drops to zero before the gate-source voltage $V_{gs(S1)}$ starts to rise and exceeds the turn-ON threshold. The converter achieves a wide gain range and excellent ZVS performance with $L_m = 600\ \mu$H.

Fig. 9(e) shows the dynamic experimental waveforms of the converter during transitions between different V_o under the same R_o. The transitions are smooth, with no voltage overshoot or current spikes, verifying the converter's stable dynamic behavior.

As shown in Fig. 9(f), the output current is initially regulated at 6 A. When R_o is decreased from 20 Ω to 12 Ω, the switching frequency f_s increases from 115 to 135 kHz to maintain CC, while the output voltage V_o decreases from 120 to 75 V. Subsequently, the current reference I_{ref} is reduced to 4 A. In response, the switching frequency further increases to 170 kHz, and the output current stabilizes at 4 A.

The efficiency results of the converter under different V_o and I_o are shown in Fig. 10(a). The L2C2 converter achieves a peak efficiency of 96.5%.

Due to the structural compatibility of the proposed L2C2 converter, the *LLC* resonant tank can be obtained by simply removing C_{r1}. After removing C_{r1}, the *LLC* converter retains the same Q and k as those defined in (7) for the L2C2 converter. As shown in Fig. 10(b), when $I_o = 6$ A, using the same design parameters, the *LLC* converter achieves a limited output voltage range of 24–70 V, with a switching frequency range of 70–350 kHz. At 350 kHz, the efficiency drops to only 82%, and below 70 kHz, ZVS cannot be maintained. In contrast, the proposed converter maintains ZVS and exhibits only a 4.2% efficiency drop over a wide output voltage range of 24–120 V. The gain range of the proposed L2C2 converter significantly exceeds that of the conventional *LLC* converter.

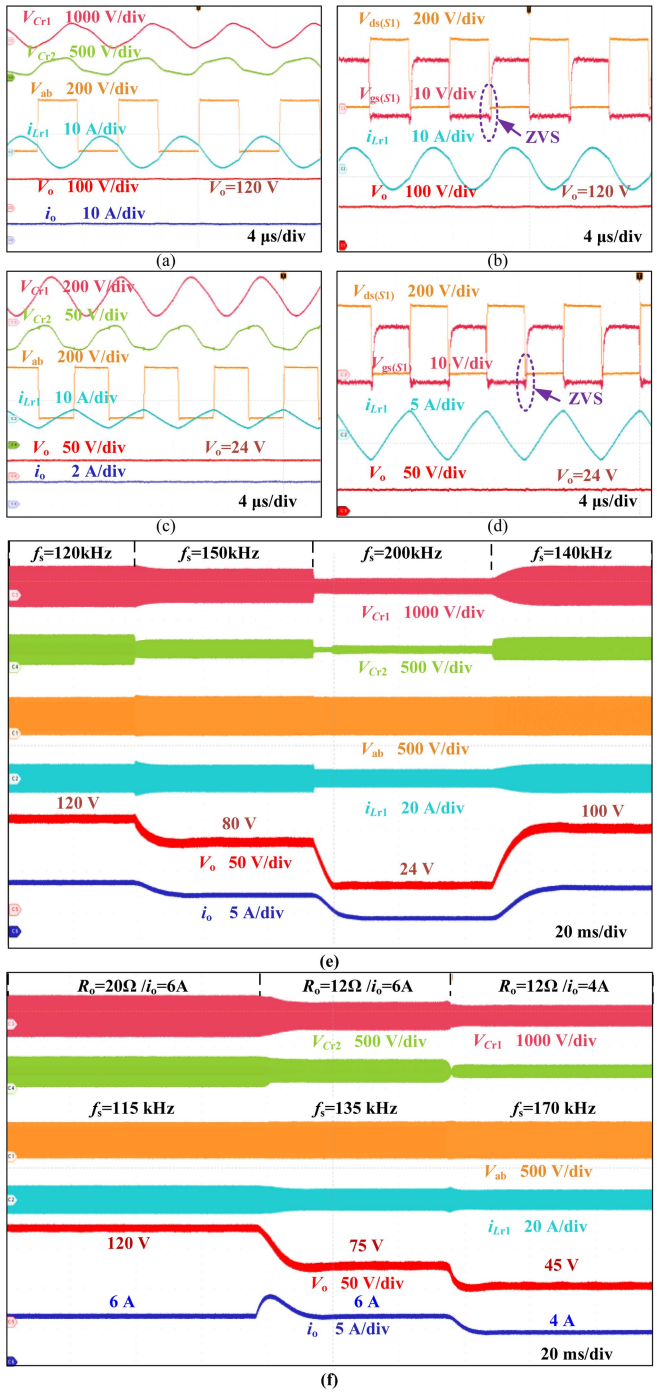

Fig. 9. Experimental results of the proposed converter. (a) Key waveforms at V_o=120 V. (b) ZVS waveforms at V_o =120 V. (c) Key waveforms at V_o =24 V. (d) ZVS waveforms at V_o =24 V. (e) Dynamic response during transitions between different V_o under constant R_o. (f) Dynamic response during transitions between different R_o and V_o.

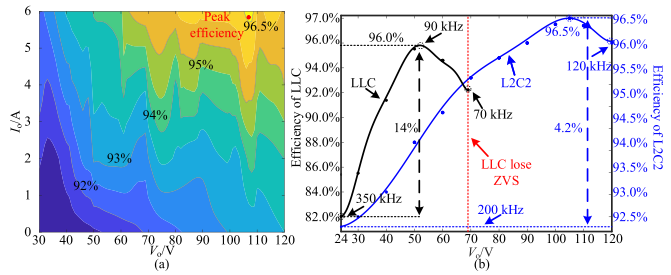

Fig. 10. Efficiency results. (a) Efficiency of L2C2 converter under different V_o and I_o. (b) Comparison between the L2C2 and *LCC* converters.

TABLE II
COMPARISON AMONG WIDE VOLTAGE RANGE TOPOLOGIES

Reference	[3]	[7]	[8]	[9]	[10]	Proposed
Topology	*B-LLC*	*CL–LLC*	*D-CLT*	*LC–LLC*	*LC–LLC*	L2C2
Switches	6	2	2	2	2	**2**
Diodes	2	4	4	2	2	**2**
Magnetic components	4	3	4	3	3	**2**
Capacitors	5	4	4	5	4	**4**
Input/output voltage(V)	24–64/ 375	400/ 350–500	400/ 20–30	25–40/ 400	330–390/ 56	400/ 24–120
V_{max}/V_{min}	2.7	1.4	1.5	1.6	1.18	**5**
Peak efficiency	94.20%	95.90%	95.20%	96%	96.38%	**96.50%**

The bolded values highlight the most outstanding performance metrics, such as the widest voltage range, the highest efficiency, or the minimal number of components, which distinguish the proposed converter from existing solutions.

The comparison results between the proposed topology and other relevant converters are presented in Table II. The proposed converter achieves a wide voltage range and high efficiency with fewer components.

As illustrated in Fig. 6, compared with the traditional *LLC* converter, the *LCC* converter achieves a wider voltage gain. However, the proposed L2C2 converter outperforms both due to its inherently higher peak and base gain, enabling the widest voltage range among the three.

In addition, while conventional *LCC* converters operate in a capacitive region without ZVS capability when the normalized frequency f_n is greater than 1, the proposed L2C2 converter maintains operation in an inductive region for $f_n > 1$, ensuring ZVS is always achievable.

The authors in [12] and [13], respectively, present two designs based on conventional *LCC* and *LLC* converters. A comparative summary of their parameters and performance is shown in Table III. The *LLC* converter has the fewest capacitors, while the total number of components in the *LCC* and *LLC* converters is similar. The proposed L2C2 converter achieves a wider gain range than both.

V. CONCLUSION

This letter presents a compact and efficient L2C2 converter with minimal modifications compared to the *LLC* converter, while offering broad gain range capability. By reducing switches, diodes, magnetics, and capacitors compared to efficient, versatile solution for various dc–dc applications. By introducing an additional resonant capacitor between the input source and the transformer, the transition from a conventional *LLC* resonant converter to the proposed L2C2 converter can be easily realized, thereby reducing implementation complexity. The gain range of the converter is positively correlated with the magnetizing inductance, allowing the inductance value to be maximized while still ensuring ZVS. A 720 W prototype is constructed to validate the operation and effectiveness of the proposed converter, demonstrating a wide output voltage.

TABLE III
COMPARISON AMONG *LCC*, *LLC*, AND L2C2 CONVERTERS

Reference	Topology	Magnetic components	Capacitors	Voltage	V_{max}/V_{min}	Peak efficiency
[12]	*LCC*	2	4	400/ 679–1000	1.6	>90%
[13]	*LCC*	2	3	365–410/ 24	1.12	95.37%
Proposed	L2C2	2	4	400/ 24–120	5	96.50%

REFERENCES

[1] T. Jin, X. S. Xiao, Z. Zhang, W. Wu, Y. Yuan, and X. Mao, "Hybrid control for three-level LLC resonant converter of dual-bridge for wide output range," *IEEE Trans. Power Electron.*, vol. 38, no. 7, pp. 8612–8623, Jul. 2023.

[2] G. Ning et al., "Dual-mode LLC converter with wide voltage gain in narrow switching frequency range," *IEEE Trans. Power Electron.*, vol. 39, no. 10, pp. 12058–12064, Oct. 2024.

[3] B. Dai, M. Su, G. Ning, H. Wang, and K. An, "Interleaved boost-integrated LC series resonant converter with frequency-free designed transformer for wide voltage range applications," *IEEE Trans. Ind. Electron.*, vol. 70, no. 8, pp. 7976–7987, Aug. 2023.

[4] Z. Hou, D. Jiao, and J.-S. Lai, "An ultrawide range pulse width modulated LLC converter with voltage multiplier rectifiers," *IEEE Trans. Power Electron.*, vol. 40, no. 4, pp. 6216–6229, Apr. 2025.

[5] R. Gu, D. Zhang, J. Duan, R. Qu, and A. Li, "Fixed-frequency circulant phase-shift controlled current-fed resonant converter with wide voltage gain range," *IEEE Trans. Ind. Electron.*, vol. 71, no. 8, pp. 8782–8792, Aug. 2024.

[6] M. Chen, B. Chen, P. Wang, Y. Wang, and M. Zhang, "A high efficiency and wide voltage gain sLC_LCC DC–DC converter with SiC devices," *IEEE Trans. Power Electron.*, vol. 38, no. 2, pp. 2169–2180, Feb. 2023.

[7] X. Zhang, J. Jing, Y. Guan, M. Dai, Y. Wang, and D. Xu, "High-efficiency high-order CL-LLC DC/DC converter with wide input voltage range," *IEEE Trans. Power Electron.*, vol. 36, no. 9, pp. 10383–10394, Sep. 2021.

[8] Y.-F. Wang, F. Han, L. Yang, C. Wang, B. Chen, and R. Xu, "A novel D-CLT multiresonant DC–DC converter with reduced voltage stresses for wide frequency variation applications," *IEEE Trans. Power Electron.*, vol. 34, no. 5, pp. 4509–4523, May 2019.

[9] H. Wu, X. Jin, H. Hu, and Y. Xing, "Multielement resonant converters with a notch filter on secondary side," *IEEE Trans. Power Electron.*, vol. 31, no. 6, pp. 3999–4004, Jun. 2016.

[10] D.-K. Kim, S. Moon, C.-O. Yeon, and G.-W. Moon, "High-efficiency LLC resonant converter with high voltage gain using an auxiliary LC resonant circuit," *IEEE Trans. Power Electron.*, vol. 31, no. 10, pp. 6901–6909, Oct. 2016.

[11] B. Chen, P. Wang, Y.-F. Wang, S.-H. Zhang, L. Yang, and R.-L. Ji, "A bidirectional CDT-LC resonant DC–DC converter with a wide voltage range," *IEEE Trans. Ind. Electron.*, vol. 67, no. 3, pp. 2009–2020, Mar. 2020.

[12] R. Wang, S. Mao, S. Yin, H. Liu, Q. Tan, and J. Fan, "Analysis and modeling of zero-voltage-switching condition for LCC resonant converter in above-resonance operation mode," *IEEE Trans. Power Electron.*, vol. 39, no. 9, pp. 10950–10961, Sep. 2024.

[13] H. Shi et al., "An LLC resonant converter with symmetric pulse-width balancing and fixed-period hysteresis burst control for high efficiency over full load range," *IEEE Trans. Power Electron.*, to be published, doi: 10.1109/TPEL.2025.3578014.